Yuzhu Song, Chang Xu, Tianyu Bai and Xiuyan Wang*

Two novel copper(II) supramolecular complexes: synthesis, crystal structures, and Hirshfeld surface analysis

https://doi.org/10.1515/zkri-2025-0031
Received June 18, 2025; accepted August 11, 2025;
published online September 3, 2025

Abstract: Under solvothermal conditions, the reaction of 3-carboxy-1-carboxymethyl-2-oxidopyridinium (H_2L), and N-donor ligands (2,2′-bipy = 2,2′-bipyridine, 4,4′-bipy = 4,4′-bipyridine) with copper(II) ions, two new complexes biaqua-bis[(μ_2-3-carboxylato-1-carboxylatomethyl-2-oxidopyridinium-κ^3 O,O′:O″)-(2,2′-bipyridine-κ^2 N,N′) copper(II)] tetrahydrate **(1)** and poly{aqua-(μ_2-3-carboxylato-1-carboxylatomethyl-2-oxidopyridinium-κ^3 O,O′:O″)-hemi(μ_2-4,4′-bipyridine-κ^2 N:N′) copper(II)] bihydrate}**(2)** have been successfully synthesized and structurally confirmed by single-crystal X-ray diffraction analysis techniques and elemental analysis. In complex **(1)**, the anionic H_2L ligand connects Cu(II) ions in a μ_2-η^1:η^1:η^1:η^0:η^0 mode to form a $[Cu(L)]_2$ unit, which is further extended into chains via π-π stacking between 2,2′-bipy ligands. Adjacent chains interconnect to form supramolecular layers through additional π-π stacking. Complex **(2)** was shown to have a chains structure in which the binuclear $[Cu(L)]_2$ moieties are linked into chains due to the bridging function of the 4,4′-bipy ligand, and further connected by hydrogen bond interactions to form a layered structure. Additionally, the properties of **(1)** and **(2)** were characterized by FT-IR, UV–vis, PL, TG and Hirshfeld surfaces analyses.

Keywords: complex; crystal structure; π-π interactions; Hirshfeld surface analysis

***Corresponding author: Xiuyan Wang**, Key Laboratory of Preparation and Applications of Environmental Friendly Materials, Jilin Normal University, Ministry of Education, Changchun 130103, China; and Department of Chemistry, Jilin Normal University, Siping 136000, China, E-mail: wangxiuyanjlnu2004@163.com
Yuzhu Song, Key Laboratory of Preparation and Applications of Environmental Friendly Materials, Jilin Normal University, Ministry of Education, Changchun 130103, China; and Department of Chemistry, Jilin Normal University, Siping 136000, China
Chang Xu and Tianyu Bai, Department of Chemistry, Jilin Normal University, Siping 136000, China

1 Introduction

Emerging as a category of functional materials, complexes formed through coordination interactions between metal ions/clusters and organic ligands have captivated significant global research interest.[1,2] Benefiting from the strong directionality of metal-ligand coordination bonds and the well-defined coordination geometries of metal centers, a wide variety of fascinating complexes with distinctive network topologies have been systematically constructed by carefully selecting metal ions and employing rational strategies for designing organic bridging ligands.[3,4] Beyond their intriguing architectures, complexes exhibit exceptional characteristics – polymetallic active sites, diverse pore sizes, high structural flexibility and tunability, facile functionalization, large adsorption capacity and ultrahigh specific surface area.[5–7] These features make promising candidates for applications in catalysis,[8,9] gas storage/separation,[10] fluorescence sensing,[11] ion exchange,[12] 3electrochemical biosensing,[13,14] and other advanced fields. Among, organic ligands play a pivotal role in the design and synthesis of complexes, where their structural diversity endows products with tailored functionalities for diverse applications.[15,16] Particularly, the mixed strategy that combines organic carboxylic acid ligands with nitrogen-containing ligands has been much more extensively studied.[17,18] The carboxylic acid ligands include rigid aromatic ligands or heterocyclic acids, as well as flexible aliphatic ligands. As a rigid ligand, 3-carboxy-1-carboxymethyl-2-oxidopyridinium provides coordination sites of varying degrees of flexibility via its carboxylic acid oxygen atoms, enabling the construction of functional complex materials with intricate architectures. Meanwhile, the linker's rigidity affords abundant hydrogen-bonding and π-π stacking interactions during extended network assembly.[19,20] Known to act as a significant class of N-donors, bipyridine (bipy) is commonly utilized in the preparation of complexes due to its strong σ-donor ability from the imine functionality and the presence of an empty, low-lying π orbital, which endows it with exceptional coordination versatility.[21–23] For example, the 2,2′-bipyridine ligand establishes compact connections with metal atoms through N,N′-chelating coordination. The

planar geometry generates open metal coordination sites that promote various intermolecular interactions, such as π-π stacking and metal-metal interactions.[24] The 4,4′-bipyridine serves as a pivotal pillar for connecting inorganic frameworks, linking metal ions through a bridging coordination mode to promote the formation of extended spatial architectures and construct stable multidimensional functional materials with enhanced structural integrity.[25,26] Jinzhong Gu et al.[27] reported two complexes: $\{[Cd(\mu\text{-Hbta})(2,2'\text{-bipy})(H_2O)]\cdot 3H_2O\}_n$ **(1)** and $[Zn_2(\mu\text{-Hbta})_2(4,4'\text{-bipy})_2(H_2O)_2]\cdot 2H_2O$ **(2)** (H_3bta = 3,2′,4′-biphenyltricarboxylic acid). In complex **(1)**, the 2,2′-bipy ligand chelates Cd(II) ions to form a six-coordinate $\{CdN_2O_4\}$ distorted octahedral geometry, distributed along wavy one-dimensional chains. In complex **(2)**, terminal N atoms of 4,4′-bipy coordinate with Zn(II) ions through a bridging mode to construct $\{ZnNO_5\}$ units, which are interconnected via hydrogen bonding to form a three-dimensional pcu network.

Herein, we investigated the self-assembly behavior of Cu(II) ions and bipyridine in conjunction with aromatic carboxylate ligands, leading to the formation of two new complexes, namely biaqua-bis[(μ_2-3-carboxylato-1-carboxylatomethyl-2-oxidopyridinium-κ^3 O,O′:O″)-(2,2′-bipyridine-κ^2 N,N′) copper(II)] tetrahydrate **(1)** and poly{aqua-(μ_2-3-carboxylato-1-carboxylatomethyl-2-oxidopyridinium-κ^3 O,O′:O″)-hemi(μ_2-4,4′-bipyridine-κ^2 N:N′) copper(II)] bihydrate}**(2)**, under solvothermal conditions. The properties of complexes **(1)** and **(2)** were thoroughly characterized, including X-ray diffraction, FT-IR, UV–vis, PL, TG and Hirshfeld surface analyses.

2 Experimental

2.1 Reagents and instruments

All reagents and chemicals used in this study were commercially sourced and utilized without further purification. Elemental analysis was performed using a Perkin-Elmer 240C analyzer. Powder X-ray diffraction (PXRD) patterns were collected using a Rigaku Dmax 2000 X-ray diffractometer equipped with graphite monochromatized CuKα radiation (λ = 0.154 nm). Thermogravimetric analysis (TGA) was carried out using a TGS DT2960 analyzer over the temperature range of 25–800 °C. The IR spectrum was recorded in the range of 4,000–400 cm^{-1} on a Perkin-Elmer Spectrum One FTIR spectrometer using a KBr pellet technique. UV–vis absorption spectra of finely ground samples were measured on a Shimadzu UV-2550 spectrophotometer, while emission spectra were recorded using a Renishaw in Via Raman microscope.

2.2 X-ray crystallography

Single crystals of complexes **(1)** and **(2)** were carefully selected for size, and single crystal X-ray diffraction analyses were performed at 273(2) K and 296(2) K on a Bruker-AXS Smart CCD diffractometer equipped with graphite-monochromatized MoKα (λ = 0.71073 Å) radiation using an ω-ϕ scan method. The structures were solved directly by SIR2014[28] and refined by the SHELXL2018/3[29] program based on F^2-based full matrix least-squares technique. All hydrogen atoms were located using difference Fourier methods and refined as riding models, while the non-hydrogen atoms were refined with anisotropic displacement parameters. The selected bond distances and angles were gathered in Table 1, and X-ray crystallographic and refinement parameters are summarized in Table 2.

2.3 Synthesis of biaqua-bis[(μ_2-3-carboxylato-1-carboxylatomethyl-2-oxidopyridinium-κ^3 O,O′:O″)-(2,2′-bipyridine-κ^2 N,N′) copper(II)] tetrahydrate (1)

$CuCl_2\cdot 2H_2O$ (0.05 mmol, 0.099 g), H_2L (0.05 mmol, 0.0099 g), and 2,2′- bipyridine (0.1 mmol, 0.0156 g) were added to H_2O

Table 1: Selected bond lengths (Å) and angles (deg) for complexes **(1)** and **(2)**.

Complex (1)			
Bond	**Value**	**Bond**	**Value**
N(2)–Cu(1)	1.986(2)	O(1W)–Cu(1)	2.328(2)
N(3)–Cu(1)	1.997(2)	O(3)–Cu(1)	1.9357(18)
O(2)–Cu(1)	1.9070(18)		
O(2)–Cu(1)–O(3)	93.95(7)	N(2)–Cu(1)–N(3)	81.15(9)
O(2)–Cu(1)–N(2)	169.11(9)	O(2)–Cu(1)–O(1W)	85.84(8)
O(3)–Cu(1)–N(2)	92.29(9)	O(3)–Cu(1)–O(1W)	91.07(8)
O(2)–Cu(1)–N(3)	91.25(8)	N(2)–Cu(1)–O(1W)	102.97(8)
O(3)–Cu(1)–N(3)	169.03(8)	N(3)–Cu(1)–O(1W)	98.94(8)
Complex (2)			
Bond	**Value**	**Bond**	**Value**
N(2)–Cu(1)	2.0222(18)	O(3)–Cu(1)	1.9533(16)
O(2)–Cu(1)	1.9203(17)	O(5)–Cu(1)^{ii}	1.9668(16)
O(1W)–Cu(1)	2.2342(19)		
O(2)–Cu(1)–O(3)	90.41(7)	O(5)^{ii}–Cu(1)–N(2)	90.80(7)
O(2)–Cu(1)–O(5)^{ii}	152.35(8)	O(2)–Cu(1)–O(1W)	105.83(8)
O(3)–Cu(1)–O(5)^{ii}	88.53(7)	O(3)–Cu(1)–O(1W)	93.32(7)
O(2)–Cu(1)–N(2)	89.33(7)	O(5)^{ii}–Cu(1)–O(1W)	101.82(7)
O(3)–Cu(1)–N(2)	178.04(7)	N(2)–Cu(1)–O(1W)	88.62(7)

Symmetry codes: ^{ii} $-x+1, -y, -z+1$.

Table 2: Crystal structure data for complexes **(1)** and **(2)**.

Complex	Complex (1)	Complex (2)
Empirical formula	$C_{36}H_{38}Cu_2N_6O_{16}$	$C_{13}H_{15}CuN_2O_8$
M_r	937.80	390.81
Temperature, K	273(2)	296(2)
Crystal size, mm^3	0.201 × 0.182 × 0.175	0.319 × 0.306 × 0.232
Crystal system	Monoclinic	Triclinic
Space group	$P2_1/n$	$P\bar{1}$
a, Å	11.7258(13)	8.7358(18)
b, Å	12.8692(14)	9.303(2)
c, Å	12.6384(14)	10.296(2)
α, °	90	68.021(3)
β, °	96.173(2)	86.161(3)
γ, °	90	76.083(3)
V, $Å^3$	1896.1(4)	753.0(3)
Z	2	2
D_{calcd}, g cm^{-3}	1.64	1.72
μ(MoKα), mm^{-1}	1.2	1.5
F(000), e	964.0	400.0
hkl range	$-13 \le h \le 12$, $-15 \le k \le 12$, $-14 \le l \le 15$	$-10 \le h \le 10$, $-9 \le k \le 11$, $-11 \le l \le 12$
Radiation wave length *λ*, Å	0.71073	0.71073
2*θ* range for data collection, °	2.25–25.01	2.13–26.10
Refl. Measured	9,130	4,264
Refl. Unique	3,306	2,963
R_{int}	0.0250	0.0142
Param. refined	275	217
$R(F)/wR(F^2)$[a,b] (all refl.)	0.0436/0.1003	0.0356/0.0866
GoF (F^2)[c]	1.089	1.052
Weighting factors A/B[b]	0.0566/0.9341	0.0482/0.5800
$\Delta\rho_{fin}$ (max/min), e°$Å^{-3}$	0.67/−0.26	0.63/−0.67
CCDC	2464040	2464039

[a] $R(F) = \Sigma||F_o| - |F_c||/\Sigma|F_o|$; [b] $wR(F^2) = [\Sigma w(F_o^2 - F_c^2)^2/\Sigma w(F_o^2)^2]^{1/2}$; $w = [\sigma^2(F_o^2) + (AP)^2 + BP]^{-1}$, where $P = (\mathrm{Max}(F_o^2, 0) + 2F_c^2)/3$;
[c] GoF = $S = [\Sigma w(F_o^2 - F_c^2)^2/(n_{obs} - n_{param})]^{1/2}$.

(2.5 mL) and DMF (3 mL) in a sealed glass vial. The resulting mixture was stirred continuously at room temperature for 15 min to get a mixed solution, followed by heating at 95 °C for 96 h. Upon cooled to room temperature, blue bulk crystal of complex **(1)** were obtained. Single crystals suitable for X-ray diffraction analysis were obtained. **(1)**: trace amount (yield~43 %, based on Cu). $C_{36}H_{38}Cu_2N_6O_{16}$ (%): calcd. C 46.11, H 4.08, N 8.96; Found C 45.27, H 4.03, N 8.73.

2.4 Synthesis of poly{aqua-(μ_2-3-carboxylato-1-carboxylatomethyl-2-oxidopyridinium-κ^3 O,O′:O″)-hemi(μ_2-4,4′-bipyridine-κ^2 N:N′) copper(II)] bihydrate}(2)

$CuCl_2{\cdot}2H_2O$ (0.1 mmol, 0.0170 g), H_2L (0.05 mmol, 0.0099 g), and 4,4′- bipyridine (0.1 mmol, 0.0160 g) were dissolved in a mixed solvent of H_2O/DMF (5 mL, 1:1 = *v*/*v*) in a glass vial. The mixture was stirred for 15 min at room temperature to ensure thorough mixing. It was then heated at 93 °C for 96 h and subsequently cooled to room temperature, yielding blue block-shaped crystals of complex **(2)**. The crystals of complex **(2)** were washed with distilled water and dried under ambient conditions. Single crystals suitable for X-ray diffraction analysis were obtained. **(2)**: trace amount (yield~38 %, based on Cu). $C_{13}H_{15}CuN_2O_8$ (%): calcd. C 39.91, H 3.38, N 7.16; Found C 39.43, H 3.82, N 7.10.

3 Results and discussion

3.1 Crystal structure description for complex (1)

The single-crystal X-ray diffraction analysis reveals that complex **(1)** crystallizes in the space group $P2_1/n$. The asymmetric unit consists of one crystallographically

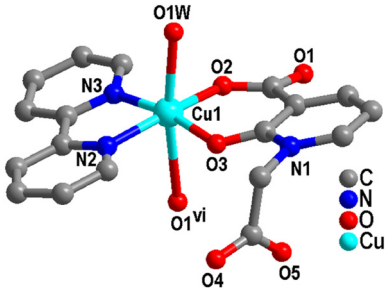

Figure 1: Coordination center of Cu(II) in complex **(1)** (Symmetric codes: [vi] 1 – *x*, –*y*, –*z*).

independent Cu(II) ion, one 2,2′-bipy ligand, one L anion, one coordinated H_2O molecule, and two free H_2O molecules. As shown in Figure 1, the coordination environment of Cu(II) ions, which exhibits a six-coordinate distorted octahedral geometry, is completed by two nitrogen atoms N(2) and N(3) (N(2)–Cu(1) = 1.986(2) Å, N(3)–Cu(1) = 1.997(2) Å) from one 2,2′-bipy ligand, three oxygen atoms O(2), O(3) and $O(1)^{vi}$ (O(2)–Cu(1) = 1.9070(18) Å, O(3)–Cu(1) = 1.9357(18) Å, Table 1) from two different L ligand anions, as well as one oxygen atom O(1W) (O(1W)–Cu(1) = 2.328(2) Å) in the H_2O molecule.

The deprotonated L ligand anion adopts a μ_2-η^1:η^1:η^1:η^0:η^0 linking mode, where the carboxylate oxygen atoms from the L ligand take the coordination mode of monodentate with adjacent Cu(II) ions, thereby forming a binuclear $[CuL]_2$ structural unit (Figure 2). The distance between adjacent Cu···Cu is 5.200 Å. Subsequently, adjacent binuclear $[CuL]_2$ clusters are interconnected through π-π stacking interactions (N(2)/C(9)–C(13), $N(2)^{vi}$/$C(9)^{vi}$–$C(13)^{vi}$; Symmetric code: [vi] 1 – *x*, –*y*, –*z*, Table 3) between the pyridine rings of the 2,2′-bipy ligands to form a supramolecular chain.[30]

Interestingly, additional π-π stacking interactions (N(3)/C(14)–C(18), $N(1)^{vii}$/$C(1)^{vii}$–$C(5)^{vii}$; Symmetric code: [vii] –1/2 – *x*, 1/2 – *y*, –1/2 – *z*) are observed between the pyridine ring of the 2,2′-bipy ligand and the aromatic ring of the H_2L ligand anion, which further extend the adjacent chains into supramolecular layers (Figure 3). The stability of the layered structure is enhanced due to the presence of O–H···O hydrogen bonds.

Table 3: The π-π interactions of complex **(1)** (Å, °).

Ring (I)···Ring (J)	Centroid tocentroid distance (Å)	*α* (°)	Slippage distance (Å)
$Cg4\cdots Cg4^{vi}$	3.7302(17)	0.02(13)	1.384
$Cg5\cdots Cg3^{vii}$	3.7898(16)	4.75(12)	1.688

Symmetry code: [vi] 1 – *x*, –*y*, –*z*; [vii] –1/2 + *x*, 1/2 – *y*, –1/2 + *z*. Ring codes – Cg3: N(1)/C(1)–C(5), Cg4: N(2)/C(9)–C(13), Cg5: N(3)/C(14)–C(18).

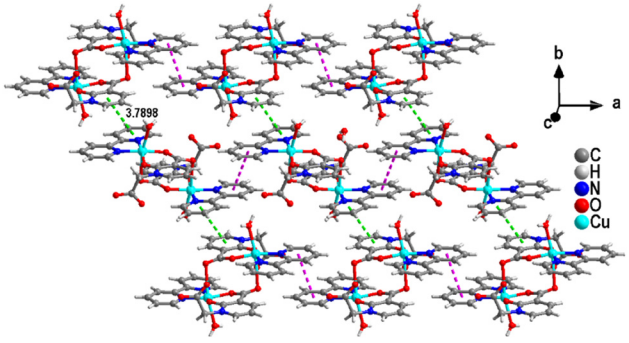

Figure 3: The layered structure of complex **(1)** formed based on another kind of π-π stacking.

3.2 Crystal structure description for complex (2)

Single crystal X-ray diffraction analysis indicates that complex **(2)** crystallizes in the triclinic system with the $P\bar{1}$ space group, exhibiting a similar layered network structure to that of complex **(2)**. As shown in Figure 4, a Cu(II) ion, a L ligand

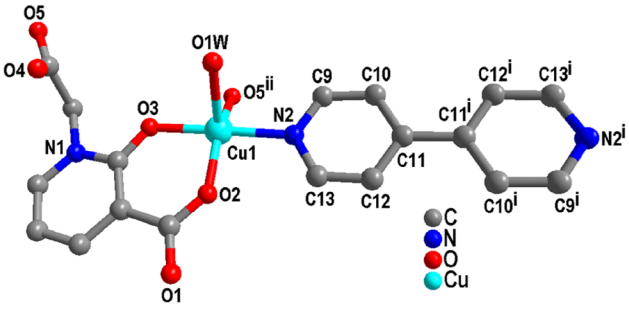

Figure 4: Coordination environment diagram of complex **(2)**.

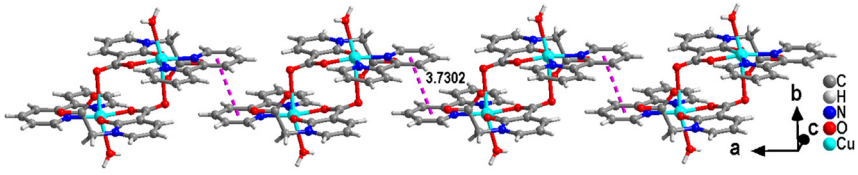

Figure 2: Complex **(1)** forms a chain through π-π interactions.

anion, half of one 4,4′-bipy ligand, a crystalline water molecule, and two free water molecules constitute the asymmetric unit structure of complex **(2)**. Each Cu(II) ion coordinates with one N atom (Cu(1)–N(2) = 2.0222(18) Å) from 4,4′-bipy, two carboxylate oxygen atoms (Cu(1)–O(2) = 1.9203(17) Å, Cu(1)–O(5)^{ii} = 1.9668(16) Å), and one hydroxyl oxygen atom (Cu(1)–O(3) = 1.9533(16) Å) from one L ligand anion, along with one oxygen atom (Cu(1)–O(1W) = 2.2342(19) Å) from a water molecule, thereby forming a five-coordinate [CuO_4N] distorted square pyramidal geometry.

As shown in Figure 5, L ligand anion connects adjacent Cu(II) ions via a μ_2-η^0:η^1:η^1:η^0:η^1 coordination mode, forming a dinuclear $[CuL]_2$ structure with a Cu⋯Cu distance of 6.710 Å. Furthermore, 4,4′-bipy bridges adjacent dinuclear $[CuL]_2$ units, generating a chain structure with an extended Cu⋯Cu distance of 11.134 Å.

Moreover, the O(1W)–H(1A)⋯O(1)^{v} hydrogen bonds facilitate the connection of chains into a layered structure (Table 4), while additional hydrogen bonds contribute significantly to the stabilization of this layered architecture (Figure 6).

3.3 Powder XRD analysis of complexes (1) and (2)

The powder X-ray diffraction (PXRD) patterns of complexes **(1)** and **(2)** are presented in Figure 7. A direct comparison reveals that the experimental diffraction peaks are in reasonable agreement with those derived from the simulated patterns, providing strong evidence for phase purity of both samples.

3.4 FT-IR spectroscopy of complexes (1) and (2)

As shown in Figure 8, infrared spectroscopy (IR) measurements of complexes **(1)** and **(2)** were conducted within the frequency range of 400–4,000 cm^{-1} using KBr as the background. Broad absorption peaks observed between 3,441 and 3,074 cm^{-1} are predominantly attributed to the hydroxyl O–H stretching vibrations of water molecules in complex **(1)**. The peak at 2,364 cm^{-1} corresponds to the stretching vibration of CO_2 from the air.[31] The characteristic peaks for C–N and C=N stretching vibrations are located at 1,653 cm^{-1} and 1,532 cm^{-1}, respectively. Additionally, two peaks at 1,592 cm^{-1} and 1,374 cm^{-1} correspond to the asymmetric ν_{as}(COO) and symmetric ν_s(COO) vibrations of the carboxylate groups in the L ligand anions. Peaks at 1,244 cm^{-1} and 1,183 cm^{-1} are assigned to the in-plane bending vibrations of C–H bonds.

In comparison with complex **(1)**, the peaks at 1,420 cm^{-1} and 1,611 cm^{-1} in complex **(2)** can be attributed to the symmetric (ν_s(COO)) and asymmetric (ν_{as}(COO)) stretching vibrations of the carboxyl group in the L ligand anions. Furthermore, the peaks at 1,648 cm^{-1}, 1,532 cm^{-1}, and 1,304 cm^{-1} are associated with the stretching vibrations of ν(C=N) and ν(C–N). The in-plane bending and out-of-plane stretching vibrations of C–H bonds are identified at 1,225 cm^{-1} and 784 cm^{-1}, respectively. Lastly, the characteristic absorption peak of Cu–O is observed at 594 cm^{-1}.[32]

3.5 Thermogravimetric analysis of complex (1) and (2)

The thermal stabilities of complexes **(1)** and **(2)** were investigated under a temperature range from 25 to 800 °C with a heating rate of 10 K min^{-1}. The weight loss profiles of complexes **(1)** and **(2)** are illustrated in Figure 9. For complex **(1)**, the first stage of weight loss occurred within the temperature range of 30–180 °C, with an actual slight weight loss of approximately 10.5 % (theoretical value: 11.51 %), which corresponded to the loss of two coordinated water molecules and four free water molecules. The second stage of weight loss began at 208 °C, where the pronounced downward trend of the thermogravimetric curve indicated the collapse of the framework structure of complex **(1)**. The curve plateaued around 550 °C, indicating that complex **(1)** was fully decomposed, leaving CuO as the final residual product. Throughout the entire process, the total weight loss amounted to 76.4 % of the initial mass. Regarding complex **(2)**, the initial weight loss observed within the temperature range of 63–171 °C can be attributed to the loss of water

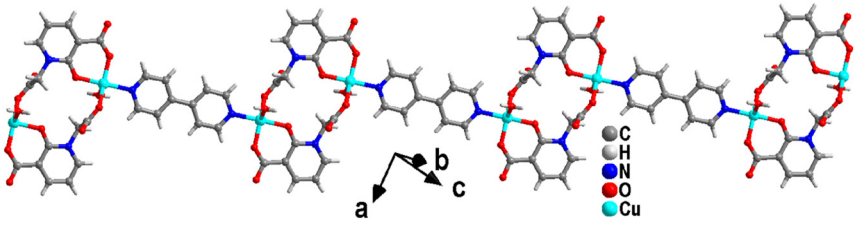

Figure 5: Chain structure of complex **(2)**.

Table 4: H-Bonding geometry parameters (Å, deg) for complexes **(1)** and **(2)**.

Complex	Donor-H···acceptor	*d*(D–H)	*d*(H···A)	*d*(D···A)	∠(DHA)
Complex **(1)**	O(1W)–H(1B)···O(2W)	0.84	2.03	2.855(3)	171.4
	O(2W)–H(2A)···O(4)^{iii}	0.85	1.96	2.805(3)	171.0
	O(2W)–H(2B)···O(3W)	0.86	2.00	2.845(3)	168.4
	O(3W)–H(3A)···O(1)	0.85	2.02	2.861(3)	169.3
	O(3W)–H(3B)···O(5)^{iv}	0.85	1.94	2.768(3)	164.3
	O(1W)–H(1A)···O(4)^{v}	0.848(10)	1.913(15)	2.744(3)	166(4)
Complex **(2)**	O(1W)–H(1A)···O(1)^{v}	0.84	2.00	2.829(2)	169.3
	O(1W)–H(1B)···O(2W)^{vi}	0.85	2.01	2.851(3)	171.7
	O(2W)–H(2A)···O(1)	0.84	1.92	2.751(3)	169.4
	O(2W)–H(2B)···O(4)^{vii}	0.85	1.96	2.805(3)	171.2
	O(3W)–H(3A)···O(4)	0.85	2.11	2.920(3)	160.3
	O(3W)–H(3B)···O(2W)^{viii}	0.85	2.04	2.882(3)	172.4

Complex **(1)**: Symmetry codes: ^{v} $-x, -y+1, -z+1$, ^{vi} $x+1, y, z$, ^{vii} $x-1, y, z$, ^{viii} $-x, -y+1, -z$. Complex **(2)**: Symmetry codes: ^{iii} $x+1/2, -y+1/2, z-1/2$, ^{iv} $-x+2, -y, -z$, ^{v} $-x+3/2, y+1/2, -z+1/2$.

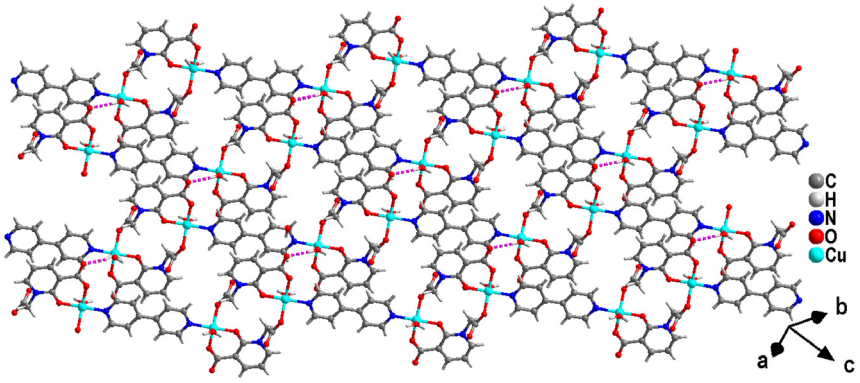

Figure 6: Structure of a complex **(2)**.

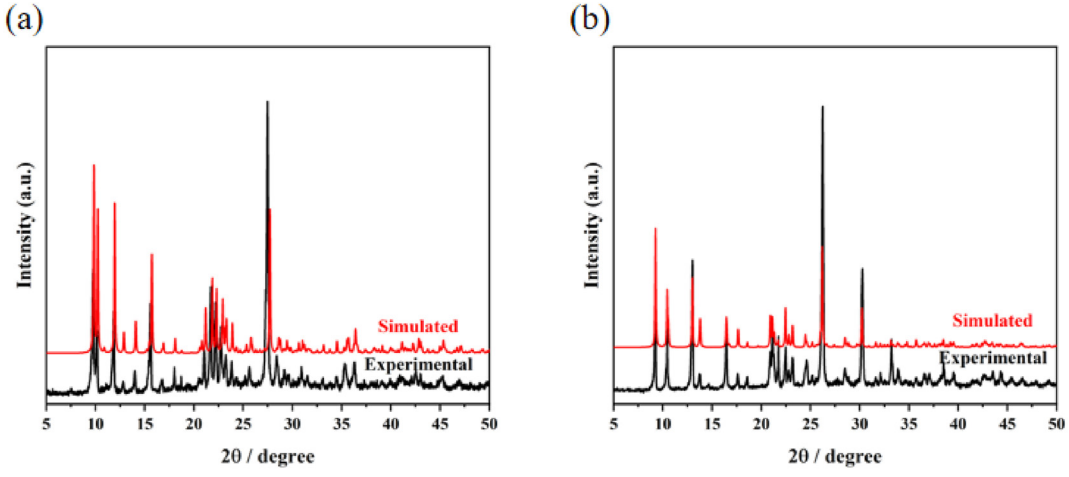

Figure 7: Experimental and simulated PXRD patterns of complexes **(1)** (a) and **(2)** (b).

molecules. A subsequent substantial weight loss was recorded between 171 and 475 °C, which is likely associated with the breakdown of the structure. The thermogravimetric curve gradually leveled off at approximately 475 °C, demonstrating that complex **(2)** had undergone complete decomposition.

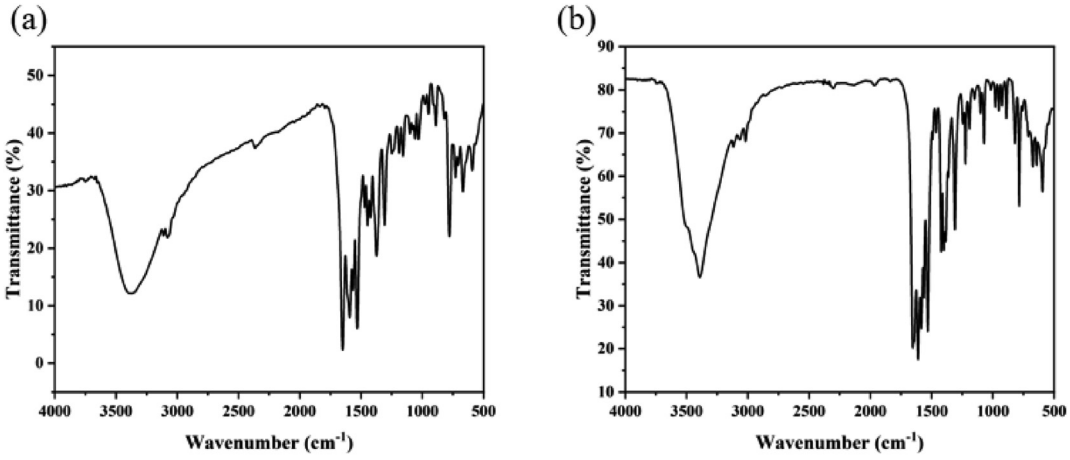

Figure 8: IR spectroscopy of complexes **(1)** (a) and **(2)** (b).

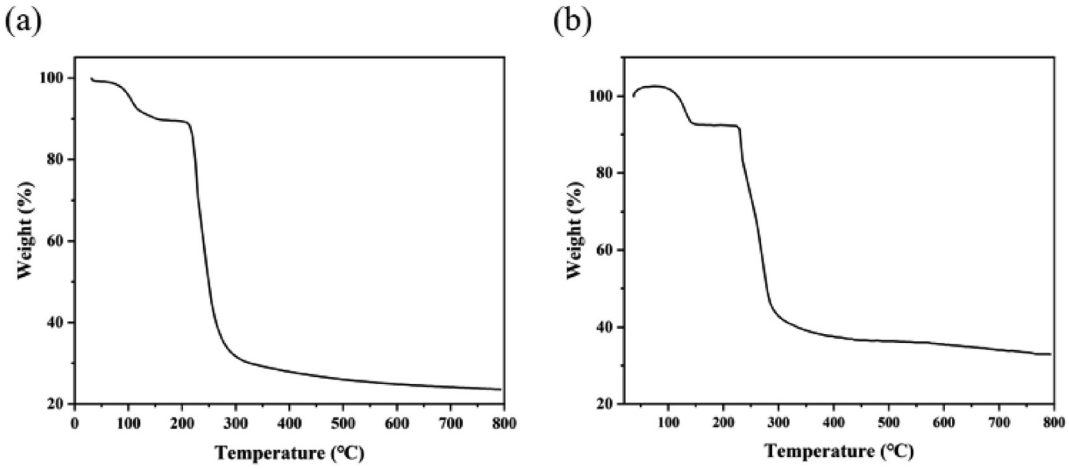

Figure 9: TG curves of the complexes **(1)** (a) and **(2)** (b).

3.6 UV–vis spectroscopy of complex (1) and (2)

Under ambient temperature conditions, the solid-state UV–Vis absorption spectra of complexes **(1)** and **(2)**, as well as their corresponding three ligands (H_2L, 2,2′-bipy and 4,4′-bipy), were measured. As shown in Figure 10(a), the 2,2′-bipy ligand exhibited high and broad absorption bands in the wavelength range of 200–267 nm, while the H_2L ligand showed similar characteristics in the 200–366 nm region. Meanwhile, the 4,4′-bipy ligand also demonstrated relatively strong absorption bands in the 200–300 nm region (Figure 10(b)). Analogous absorption features were observed for complexes **(1)** and **(2)**: complex **(1)** displayed absorption bands in the 200–339 nm range, whereas complex **(2)** exhibited absorption in the narrower 200–258 nm region. These absorption bands are predominantly attributed to π-π^* and n-π^* transitions within the ligands. Furthermore, the absorption bands of complex **(1)** in the 470–800 nm region, along with the strong absorption band of complex **(2)** within the same spectral range, can be ascribed to the d-d transitions of the Cu^{2+} centers.[33]

3.7 Photoluminescence spectroscopy of complex (1) and (2)

The solid-state photoluminescence characteristics of complexes **(1)** and **(2)**, along with the organic ligands H_2L, 2,2′-bipy and 4,4′-bipy, were recorded. As depicted in Figure 11(a), the H_2L ligand exhibited a pronounced emission peak at 383 nm under an excitation wavelength of 256 nm, whereas the 2,2′-bipy ligand showed emission peaks at 377 nm (λ_{ex} = 330 nm). Remarkably, complex **(1)** displayed a

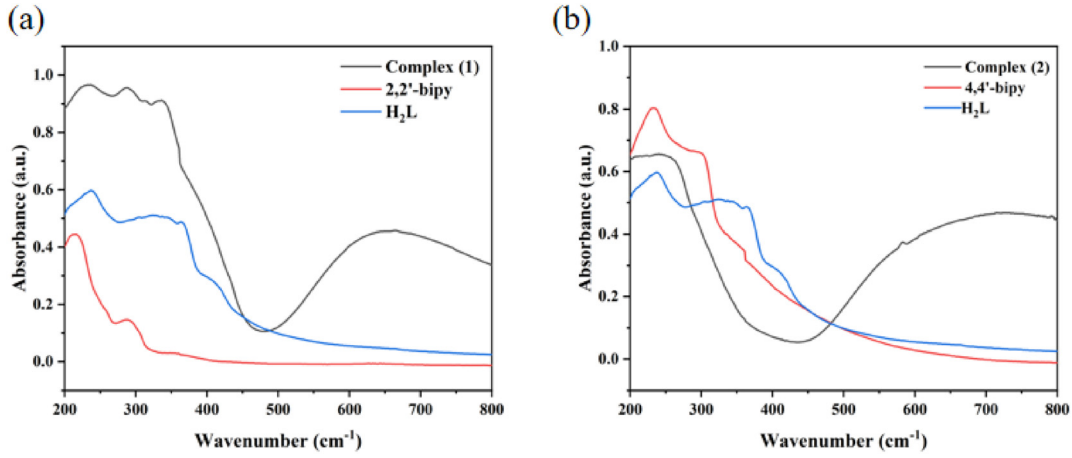

Figure 10: UV–vis spectroscopy of complexes **(1)** (a) and **(2)** (b).

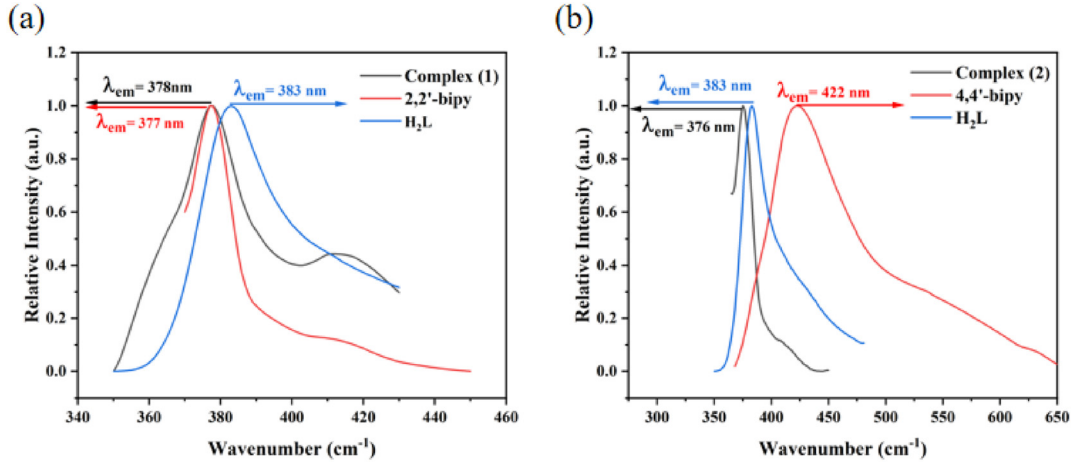

Figure 11: The solid-state photoluminescence spectra: complex **(1)**, 2,2′-bipy and H_2L ligand (a); complex **(2)**, 4,4′-bipy and H_2L ligand (b).

robust emission at 378 nm (λ_{ex} = 327 nm), which closely overlapped with the emission profile of the 2,2′-bipy ligand. This spectral congruence implies that the fluorescence emission of complex **(1)** likely arises from intraligand charge transfer within the 2,2′-bipy ligand. In Figure 11(b), the 4,4′-bipy and H_2L ligands exhibited emission bands at 422 nm (λ_{ex} = 256 nm) and 383 nm (λ_{ex} = 329 nm), respectively. Under 329 nm excitation, complex **(2)** displayed a strong emission band at 376 nm, closely matching the H_2L ligand's profile, which indicates intraligand charge transfer (ILCT) within the H_2L ligand.[34]

3.8 Hirshfeld surface analysis of complex (1)

Hirshfeld surfaces analyzed for complex **(1)** were generated using CrystalExplorer21.5[35] and the d_{norm}, shape-index, and curvedness parameters were obtained, complemented by fingerprint plot analysis. The d_{norm} color mapping reflects interatomic distances: red regions denote intermolecular distances shorter than the sum of van der Waals radii, white areas represent approximate van der Waals contacts, and blue zones indicate distances exceeding the van der Waals sum. Figure S1 shows multiple bright and light-red spots on the d_{norm} surface, attributed to hydrogen-bonding interactions. The shape-index surface reveals distinct π-π stacking interactions, characterized by adjacent red-yellow and blue-green triangular patterns alongside back-to-back diamond motifs. The curvedness analysis highlights surface flatness correlated with molecular packing efficiency.

The two-dimensional fingerprint plots in Figure S2 depict the corresponding percentage contributions of intermolecular contacts within complex **(1)**. Among these, H···H intermolecular contacts exhibit the highest contribution at 37.9 %, while O···H/H···O interactions account for a significant 29.9 % of the overall crystal packing. C···H/H···C interactions

contribute 14.7 % to the surface area. Other weak intermolecular contacts make minor contributions, including C···C (7.6 %), H···N/N···H (3.7 %), C···O/O···C (1.9 %), O···Cu/Cu···O (1.5 %), O···O (1.1 %), and N···O/O···N (1.1 %).

4 Conclusions

In summary, we synthesized two Cu(II)-based complexes: biaqua-bis[(μ_2-3-carboxylato-1-carboxylatomethyl-2-oxidopyridinium-κ^3 O,O′:O″)-(2,2′-bipyridine-κ^2 N,N′) copper(II)] tetrahydrate **(1)** and poly{aqua-(μ_2-3-carboxylato-1-carboxylatomethyl-2-oxidopyridinium-κ^3 O,O′:O″)-hemi(μ_2-4,4′-bipyridine-κ^2 N:N′) copper(II)] bihydrate}**(2)** their structures and properties were studied carefully. The results show that both complexes exhibit a layered structure. The distinct coordination modes of nitrogen atoms from the two kinds of bipyridine ligands lead to complex **(1)** adopting a six-coordinate distorted octahedral geometry, while complex **(2)** assumes a five-coordinate distorted square pyramidal structure. In complex **(1)**, the binuclear $[Cu(L)]_2$ units are further interconnected via two distinct types of π-π stacking interactions, thereby forming a layered structural framework. For complex **(2)**, adjacent Cu(II) ions are bridged by the L ligand anion in a μ_2-η^0:η^1:η^1:η^0:η^1 coordination mode, forming dinuclear $[Cu(L)]_2$ units that are further linked into chains through 4,4′-bipy ligands. These chains are ultimately extended into layers via hydrogen bonding interactions.

Research ethics: Not applicable.
Informed consent: Not applicable.
Author contributions: All authors have accepted responsibility for the entire content of this manuscript and approved its submission.
Use of Large Language Models, AI and Machine Learning Tools: None declared.
Conflict of interest: The authors state no conflict of interest.
Research funding: This work was supported by the Natural Science Fund Program of Jilin Province (No. 20240101148JC).
Data availability: The datasets generated during and/or analyzed during the current study are available from the corresponding author on reasonable request.

References

1. Ma, Z. L.; Wang, M. C.; Tian, L.; Cheng, L. A Multi-Responsive Luminescent Indicator Based on a Zn(II) Metal-organic Framework with “Turn On” Sensing of Pyridine and “Turn Off” Sensing of Fe^{3+}, $Cr_2O_7^{2-}$ and Antibiotics in Aqueous Media. *Inorg. Chim. Acta* **2021**, *526*, 120513.
2. Wang, H. L.; Liu, K. M.; Kong, Z. G.; Zhao, L. N.; Zhang, H. A Cu(II) Coordination Compound Constructed by Mixed Ligands of 1,10-phenanthroline and Carboxylic Acid: Synthesis, Characterization and Hirshfeld Surface Analysis. *Bull. Chem. Soc. Ethiop.* **2025**, *39* (3), 437–446.
3. Wang, X. Y.; Lu, H.; Huang, K. L.; Zhang, C. P.; Tian, F.; He, M. Y.; Chen, S. C.; Chen, Q. Synthesis; Characterization, Ion-Exchange, and Catalytic Properties of Three Isostructural Copper(II) Coordination Polymers with a Flexible Bis(Triazole) Ligand. *J. Solid State Chem.* **2022**, *312*, 123201.
4. Jiang, M.; Weng, Y. G.; Zhou, Z. Y.; Ge, C. Y.; Zhu, Q. Y.; Dai, J. Cobalt Metal-Organic Frameworks Incorporating Redox-Active Tetrathiafulvalene Ligand: Structures and Effect of LLCT Within the MOF on Photoelectrochemical Properties. *Inorg. Chem.* **2020**, *59* (15), 10727–10735.
5. Wen, Q.; Chen, J. L.; Song, J. F.; Zhou, S. Y.; Zhu, H. Y.; Zhang, X. Q. Synthesis of Novel Coordination Polymer Cd-MOF and Fluorescent Probe Detection of Fe^{3+}, $Cr_2O_7^{2-}$, and Ceftriaxone Sodium(CRO). *J. Mol. Struct.* **2024**, *1300*, 137235.
6. Yu, S. F.; Ma, L. S.; Liu, C. L. Two Cd(II) Complexes: Fluorescence Performances and Loaded with Paclitaxel-Hydrogel on Oral Cancer Treatment. *Inorg. Chim. Acta* **2024**, *571*, 122227.
7. Demir, S.; Dikmen, G.; Erer, H. 2D Cadmium(II) Coordination Polymer Based on 2,5-Furandicarboxylate and 1,4-Bis(1H-imidazol-1-yl)butane Linkers: Synthesis, Characterization and DFT Studies. *J. Inorg. Organomet. Polym. Mater.* **2024**, *34* (9), 4203–4213.
8. Lee, C. Y.; Ye, Y. H.; Wang, S. W.; Chen, J. D. Diverse Co(II) Coordination Polymers with the Same Mixed Ligands: Evaluation of Chemical Stability and Structural Transformation. *Molecules* **2024**, *29* (8), 1748.
9. Wang, H. L.; Li, S.; Zhang, H.; Su, B. H.; Wang, X. Y. Syntheses, Crystal Structures, and Characterizations of Two New Zn(II)/Ni(II) Coordination Polymers Constructed by N-donor Ligands and Sulfate-Bridge. *Main Group Met. Chem.* **2025**, *48* (1), 20240029.
10. Wu, M. Z.; Shi, J. Y.; Chen, P. Y.; Li, T. A Three-Dimensional Cd(II) Metal-Organic Framework: A Bifunctional Luminescence Sensor for Benzaldehyde and Fe^{2+} Ions. *New J. Chem.* **2019**, *43* (26), 10575–10582.
11. Xue, Y. S.; Zhang, X. Y.; Tian, Z. C.; Cao, J. R.; Wang, W. J.; Tang, R. X.; Wang, J.; Fei, Z. H. A Ni(II) Coordination Polymer as a Multifunctional Luminescent Sensor for Detection of UO_2^{2+}, $Cr_2O_7^{2-}$, CrO_4^{2-} and Nitrofurantoin. *Molecules* **2023**, *28* (12), 4673.
12. Sun, S. L.; Sun, X. Y.; Sun, Q.; Gao, E. Q. Highly Efficient Fluorescent Chemosensor for Nitro Antibiotic Detection Based on Luminescent Coordination Polymers with 2,6-di(4-carboxyphenyl)pyrazine. *CrystEngComm* **2021**, *23* (17), 3167–3174.
13. García-Valdivia, A. A.; Zabala-Lekuona, A.; Ramírez-Rodríguez, G. B.; Delgado-López, J. M.; Fernández, B.; Cepeda, J.; Rodríguez-Diéguez, A. 2D-coordination Polymers Based on 1H-indazole-4-carboxylic Acid and Transition Metal Ions: Magnetic, Luminescence and Biological Properties. *CrystEngComm* **2020**, *22* (30), 5086–5095.
14. Dun, L. N.; Zhang, B. S.; Wang, J. J.; Wang, H.; Chen, X.; Li, C. B. Crystal Structure, Synthesis and Luminescence Sensing of a Zn(II) Coordination Polymer with 2,5-dihydroxy-1,4-terephthalic Acid and 2,2′-bipyridine as Ligands. *Crystals* **2020**, *10* (12), 1105.
15. Köse Yaman, P.; Demir, O.; Demir, S.; Zeyrek Ongun, M.; Oğuzlar, S.; Erer, H. Sensitivity to NH_3 Vapor: Synthesis and Characterization of Five New Coordination Polymers Based on 2,2-Dimethylglutaric Acid and Bis(triazole)-derived Ligands. *ACS Omega* **2024**, *9* (3), 3193–3203.
16. Li, F. F. A New Zn(II) Two-Dimensional Coordination Polymer: Synthesis, Structure, Highly Efficient Fluorescence and DFT Study. *Acta Chim. Slov.* **2022**, *69* (3), 596–603.

17. Hu, Z. F.; Chai, Z. L.; Zhou, Q.; Feng, L. C.; Dong, W. K.; Ding, Y. J. The First Salamo-Type Mixed-Ligand Cu(II) Coordination Polymer: Synthesis, Crystal Structure and Theoretical Studies. *J. Mol. Struct.* **2023**, *1287*, 135709.
18. Tian, F.; Shen, N.; Chen, S. C.; Jiang, L. T.; Chen, Q.; He, M. Y. Syntheses, Structures, and Catalytic Properties of Three Copper(II) Coordination Polymers Based on 2,3,5,6-Tetrafluoro-1,4-Bis(triazole-ylmethyl) benzene and Benzene Carboxylate Ligands. *Z. Anorg. Allg. Chem.* **2019**, *645* (1), 57–63.
19. Li, J.; Ren, H. J.; Li, J. T.; Wang, L. C. Two Triazole-based Coordination Polymers: Synthesis and Crystal Structure Characterization. *Open Chem*. **2024**, *22* (1), 20230211.
20. Li, X. M.; Huang, Y. J.; Liu, B.; Wang, X. Y. A Zinc(II) Polymer Constructed with 3,5-Pyrazoledicarboxylic Acid and 1,4-Bis(imidazol-1-ylmethyl) butane: Syntheses, Crystal Structures, and Photoluminescence Properties. *Main Group Met. Chem.* **2025**, *48* (1), 20240013.
21. Al-Matarneh, M. C.; Nicolescu, A.; Dascalu, I. A.; Shova, S.; Varganici, C. D.; Fifere, A.; Marinas, I. C. Synthesis of New Zinc and Copper Coordination Polymers Derived from Bis(Triazole) Ligands. *Crystals* **2024**, *14* (2), 144.
22. Rojas Perez, Y.; Slep, L. D.; Etchenique, R. Cis-Trans Interconversion in Ruthenium(II) Bipyridine Complexes. *Inorg. Chem.* **2019**, *58* (17), 11606–11613.
23. Xue, S. F.; Guo, Y. N.; Rotaru, A.; Müller-Bunz, H.; Morgan, G. G.; Trzop, E.; Collet, E.; Oláh, J.; Garcia, Y. Spin Crossover Behavior in a Homologous Series of Iron(II) Complexes Based on Functionalized Bipyridyl Ligands. *Inorg. Chem.* **2018**, *57* (16), 9880–9891.
24. Iwai, T.; Abe, S.; Takizawa, S. Y.; Masai, H.; Terao, J. Insulated π-conjugated 2,2′-bipyridine Transition-Metal Complexes: Enhanced Photoproperties in Luminescence and Catalysis. *Chem. Sci.* **2024**, *15* (23), 8873–8879.
25. Chen, W. T. Photoluminescence, Semiconductive Properties and TDDFT Calculation of a Novel Cadmium Bipyridine Complex. *Inorg. Nano-Metal Chem.* **2020**, *50* (6), 453–458.
26. Morozov, A. N.; Popov, L. D.; Tkachev, V. V.; Raspopova, E. A.; Chetverikova, V. A.; Lyubchenko, S. N.; Shilov, G. V. Synthesis and Crystal Structure of 2D Coordination Polymer $\{[Cu(dps)_2(DMSO)_2](ClO_4)_2\}_n$ Based on 4,4′-Dipyridyl Sulfide. *Russ. J. Gen. Chem.* **2019**, *89*, 82–86.
27. Gu, J. Z.; Wan, S. M.; Dou, W.; Kirillova, M. V.; Kirillov, A. M. Coordination Polymers from an Unexplored Biphenyl-Tricarboxylate Linker: Hydrothermal Synthesis, Structural Traits and Catalytic Cyanosilylation. *Inorg. Chem. Front.* **2021**, *8* (5), 1229–1242.
28. Burla, M. C.; Caliandro, R.; Carrozzini, B.; Cascarano, G. L.; Cuocci, C.; Giacovazzo, C.; Mallamo, M.; Mazzone, A.; Polidori, G. Crystal Structure Determination and Refinement via SIR2014. *J. Appl. Crystallogr.* **2015**, *48* (1), 306–309.
29. Sheldrick, G. M. Crystal Structure Refinement with SHELXL. *Cryst. Struct. Commun.* **2015**, *71* (1), 3–8.
30. Zhu, Y. Y.; Li, J. T.; Gu, J. M.; Kan, L.; Liu, Y. L. A Three-Dimensional Cu-MOF with Strong π-π Interactions Exhibiting High Water and Chemical Stability. *Inorg. Chem. Commun*. **2019**, *99*, 108–112.
31. Wang, C. L.; Zhang, J. Y.; Li, X. Y.; Ren, N.; Zhang, J. J. Crystal Structure, Thermodynamic Behavior, and Luminescence Properties of a New Series of Lanthanide Halogenated Aromatic Carboxylic Acid Complexes. *Arabian J. Chem.* **2022**, *15* (9), 104089.
32. Hasanova, S. S.; Yolchueva, E. A.; Mashadi, A. Q.; Muhammad, S.; Ashfaq, M.; Muhammed, M. E.; Munawar, K. S.; Tahir, M. N.; Sehemi, A. G.; Alarfaji, S. S. Synthesis, Characterization, Crystal Structures, and Supramolecular Assembly of Copper Complexes Derived from Nitroterephthalic Acid Along with Hirshfeld Surface Analysis and Quantum Chemical Studies. *ACS Omega* **2023**, *8* (9), 8530–8540.
33. Jiao, S. S.; Zhang, Y. W.; Zhang, X. H.; Liu, K.; Ma, D. X.; Yang, B.; Li, S. X.; Wang, L. Construction, Structure Diversity, Luminescent and Dye Absorption Properties of Coordination Polymers Comprising Semi-rigid 6-(carboxymethoxy)-2-naphthoic Acid. *J. Solid State Chem.* **2021**, *293*, 121773.
34. Chen, D.; Li, X.; Wang, Y. X.; Xue, J. P. Series of Fluorescent Coordination Polymers Exhibiting Structural Evolution and Optimized Selective Ion Detection. *Cryst. Growth Des.* **2025**, *25* (5), 1497–1505.
35. Spackman, P. R.; Turner, M. J.; McKinnon, J. J.; Wolff, S. K.; Grimwood, D. J.; Jayatilaka, D.; Spackman, M. A. CrystalExplorer: A Program for Hirshfeld Surface Analysis, Visualization and Quantitative Analysis of Molecular Crystals. *J. Appl. Crystallogr.* **2021**, *54*, 1006–1011.

Supplementary Material: This article contains supplementary material (https://doi.org/10.1515/zkri-2025-0031).